This article has been accepted for publication in a future issue of this journal, but has not been fully edited. Content may change prior to final publication. Citation information: DOI 10.1109/TAES.2017.2775924, IEEE Transactions on Aerospace and Electronic Systems

Lagrange polynomial interpolation based Keystone Transform for passive radar

F. Pignol, F. Colone, T. Martelli

Dept. of Information Engineering, Electronics and Telecommunications (DIET),
Sapienza University of Rome, Via Eudossiana, 18 - 00184 Rome, Italy

***Abstract*— In this paper we address the problem of target's range migration in passive bistatic radar exploiting long coherent integration times with fairly wideband signals of opportunity. We resort to the well-known Keystone Transform (KT) to compensate for the range walk effect and to take advantage of a higher coherent integration gain against targets with non-negligible radial velocity. Specifically, an efficient implementation of the KT is proposed, based on Lagrange polynomial interpolation, in order to reduce the computational load of the method that mostly depends on the required slow-time interpolation stage. The analysis conducted against simulated data shows that the conceived approach allows to achieve theoretical performance while further reducing the KT complexity with respect to alternative solutions based on cardinal sine functions or Chirp-Z Transforms. Moreover, the application against experimental data sets collected by a DVB-T based passive radar proves the practical effectiveness of the proposed algorithm and highlights its suitability for real-time air traffic surveillance applications.**

***Index Terms*—Keystone Transform, Long coherent integration time, Passive radar, Range migration compensation.**

I. INTRODUCTION

By exploiting illuminators of opportunity, passive radar (PR) might suffer from a limited coverage since the radiative characteristics of the selected transmitter (i.e. power level, antenna pattern shape) could be inadequate to fulfill the requirements on the resulting radar system [1]. However, the stationary nature and the isotropic characteristic of many of the employable transmitters potentially allow to exploit very long integration times on receive to compensate for the limited power density provided by the emitter. This certainly applies to many ground-based transmitters for analog or digital radio/TV broadcasting. By continuously emitting their signals, these transmitters provide a persistent illumination of the target of interest.

Both coherent and non-coherent integration strategies could be considered to exploit such long observation times [2]-[3]. In both cases, in order to actually benefit of an extended integration time, possible range and Doppler walk effects should be compensated for, with a non-negligible impact on the computational complexity of the PR signal processing chain. The occurrence and the severity of range/Doppler walk effects are largely dependent on the considered surveillance application as well as on the employed waveform of opportunity. In fact, the surveillance application sets the typical motion parameters for targets of interest (e.g. maximum speed, acceleration, etc.). The carrier frequency and the bandwidth of the employed waveform define the velocity resolution and range resolution for the resulting PR system.

In this paper, we refer to the case of a DVB-T based PR for air traffic surveillance. In this application, the performance of such system suffers from the limited coherent integration time (CIT) employed in practice to avoid target range/Doppler migration, at the same time containing the computational burden [4]-[5]. Basically, DVB-T based PR has been shown to allow a reliable detection capability against targets at distances up to a few tens of kilometers [1], [6]-[8]. Typically, in the considered application, a CIT in the order of 0.1 seconds is adopted when a conventional Cross-Ambiguity Function (CAF) is employed at the detection stage. Such limit is mostly due to the range walk effect caused by the high speed of the aircrafts (up to 240 m/s) compared to the reasonably narrow range resolution cell (about 20 m equivalent monostatic range resolution). Aiming to the detection of low RCS aircrafts or to the widening of the coverage area, the possibility of extending the CIT has to be considered by properly correcting the range migration effect.

In recent years, by taking inspiration from original algorithms defined for active radar systems, different approaches have been proposed to counteract this problem in PR systems. In [9]-[10] a generalized CAF was introduced, based on the time scaling or 'stretching' of the reference signal. When applied against discrete signals, this 'stretching' can be considered as a resampling so it can be efficiently performed by exploiting a chirp z-transform (CZT). Nevertheless, this approach could be computationally intensive as the resampling has to be, in principle, repeated at each Doppler cell. In fact sub-optimal schemes were also suggested where the stretching was performed just once for each group of neighboring Doppler cells [9]-[10] or on different signal fragments of limited duration in [11].

Alternatively, the keystone transform (KT) is commonly used to compensate for range migration in active radar systems [12]-[14]. It has been applied also to the PR case in [15]-[21]

This article has been accepted for publication in a future issue of this journal, but has not been fully edited. Content may change prior to final publication. Citation information: DOI 10.1109/TAES.2017.2775924, IEEE Transactions on Aerospace and Electronic Systems

where a Batches Algorithm architecture [22]-[23] is employed to recreate the classical slow-time/fast-time framework of a pulsed radar operating at a given pulse repetition frequency (PRF). The KT also involves a computationally intensive resampling stage in the slow-time domain. However, different approaches have been devised aiming at reducing the computational load with respect to a conventional sinus cardinal interpolation (SCI). In [24], the SCI was replaced by the CZT, which was shown to lower the computational complexity while providing optimal performance. Such approach has been then applied to the PR case in [21].

A reasonable alternative is provided by the Lagrange *P*-order polynomial interpolation (*P*-LPI) whose possible application for the active radar case has been preliminary investigated in [25]. Basically only *P*+1 consecutive samples in the slow-time domain are exploited to evaluate the interpolated samples according to a *P*-order polynomial. Only the case of a linear interpolation (namely a 1-LPI) has been recently considered for the PR case in [17].

In this paper we show that the *P*-LPI method is very well suited for the PR case and provides a flexible tool to be employed within a KT stage. In fact, being the interpolation based on a limited number of samples, this method could be computationally effective whilst intrinsically sub-optimal. However, the expected loss can be traded for a reduced computational load. Moreover we show that the expected loss can be largely controlled by properly selecting both the order *P* of the polynomial and the system equivalent PRF resulting from the batching strategy. Notice that, in PR system, the latter parameter is not subject to severe constraints on range and Doppler ambiguities. In contrast its setting is typically regulated by the requirements on SNR loss and computational load [22]-[23]. Therefore, by properly acting on this parameter, we show that, even operating with a limited order *P*, negligible loss should be accepted with respect to the application of a SCI or a CZT based interpolations, with a significant computational load saving.

To this purpose, we significantly extent the studies in [25][17] by evaluating the theoretical performance of a *P*-LPI-based KT as a function of the employed order *P* and the batches duration. By defining proper performance metrics, the analysis includes the study of the Signal to noise Ratio (SNR) loss, the control of sidelobes level in the resulting range/Doppler map, and the computational load.

Based on the performed analysis, an appropriate selection of the relevant parameters is considered and the algorithm is extensively applied against experimental data sets provided by Leonardo S.p.A. in the framework of a long-term collaboration with the research group at Sapienza University of Rome. The experimental results clearly demonstrate the benefits of the extended CIT in DVB-T based PR allowed by KT range migration compensation. In particular it is shown that comparable target detection capability is obtained after the proposed *P*-LPI based KT with respect to an optimal CZT based KT, while requiring significantly reduced computational times.

The paper is organized as follows. In Section II, the problem is formulated and the limits on the CIT are evaluated for typical geometries by taking into account the different migration effects. In Section III we discuss the application of the KT in the passive radar case by identifying its peculiar characteristics and benefits. The various interpolation strategies are introduced in Section IV where the metrics adopted for their performance comparison are also illustrated. The comparative analysis of such performance is conducted in Section V against simulated data and significantly extended in Section VI against the experimental data sets available. Finally our conclusions are drawn in Section VII.

II. Problem Formulation and Limits on the Coherent Integration Time

According to a basic PR processing scheme, after disturbance removal at the surveillance channel, target detection is sought by evaluating the bistatic delay/Doppler Cross-Ambiguity Function (CAF) between the surveillance signal, $s(t)$, and the reference signal, $r(t)$:

$$\chi[l,m] = \sum_{n=0}^{N_{CIT}-1} s[n] r^*[n-l] \exp\left(-j2\pi \frac{mn}{N_{CIT}}\right) \qquad (1)$$

where N_{CIT} is the number of integrated samples, l is the delay bin and m is the Doppler bin.

As it is well known, when the signal is sampled at Nyquist rate, the evaluation of the CAF allows a coherent integration gain equal to the number of integrated samples if the target echoes collected within the CIT remain within the same bistatic range/Doppler resolution cell. This constraint sets an upper bound to the employable CIT, $T_{CIT,}$ i.e.

$$T_{CIT} \le \bar{T}_{CIT} = \min\left\{\bar{T}_{CIT}^{(R)}, \bar{T}_{CIT}^{(D)}\right\} \qquad (2)$$

being $\bar{T}_{CIT}^{(R)}$ and $\bar{T}_{CIT}^{(D)}$ the maximum CIT allowed without experiencing range and Doppler walk effects, respectively.

In the following we show that, in the considered air surveillance application, assuming a uniform motion for the target, the tightest constraint in eq. (2) is usually provided by the need to avoid range migration (i.e. $\bar{T}_{CIT} = \bar{T}_{CIT}^{(R)}$).

In fact we recall that DVB-T signals employ an orthogonal frequency division multiplexing (OFDM) modulation with a bandwidth of approximately 8 MHz, which yields a bistatic range resolution $\Delta R_{res} \cong 40m$. Therefore $\bar{T}_{CIT}^{(R)}$ is evaluated as:

$$\bar{T}_{CIT}^{(R)} = \max\left\{T_{CIT} \;\middle|\; \Delta R_B(T_{CIT}) < \frac{\Delta R_{res}}{K}\right\} \qquad (3)$$

where *K* identifies a proper fraction of the range resolution cell in order to avoid significant integration loss. $\Delta R_B(T_{CIT})$ is the largest variation of the target bistatic range $R_B(t)$ during the CIT, i.e. $\Delta R_B(T_{CIT}) = \max\big(R_B(t)\big) - \min\big(R_B(t)\big)$ with $|t| < \frac{T_{CIT}}{2}$. The time-varying target bistatic range is given by:

$$R_B(t) = \|\boldsymbol{P}_{TX} - \boldsymbol{P}(t)\| + \|\boldsymbol{P}_{RX} - \boldsymbol{P}(t)\| \qquad (4)$$

where $\boldsymbol{P}_{Tx}$ and $\boldsymbol{P}_{Rx}$ are the vectors representing the transmitter (Tx) and the PR receiver (Rx) positions in 3D space. Similarly,

This article has been accepted for publication in a future issue of this journal, but has not been fully edited. Content may change prior to final publication. Citation information: DOI 10.1109/TAES.2017.2775924, IEEE Transactions on Aerospace and Electronic Systems

$\boldsymbol{P}(t)$ represents the target time-varying position; assuming a constant velocity motion model, it can be written as $\boldsymbol{P}(t) = \boldsymbol{P}(0) + \boldsymbol{v}t$, being $\boldsymbol{v}$ the target velocity vector.

As an example, Figure 1 reports the results provided by eq. (3) as a function of the target position at t=0, i.e. $\boldsymbol{P}(0)$. In the reported example, $\boldsymbol{P}_{Rx}$ coincides with the origin of the axes, the Tx antenna is at $\boldsymbol{P}_{Tx}$ =(-10 km,0,0)^T, and the results are provided on the region with bistatic range in the interval [20km, 100km]. Moreover, the target velocity vector has modulus $\|\boldsymbol{v}\|$=100 m/s and lies on a horizontal plane, forming with the x-axis an angle ϕ. Accordingly, at each target position $\boldsymbol{P}(0)$, the maximum allowed CIT is reported in Figure 1 for the worst case condition, i.e. for the direction ϕ providing the tightest constraint. The target is assumed to fly at height H=5 km, and the value of K in eq. (3) has been set to K=1.

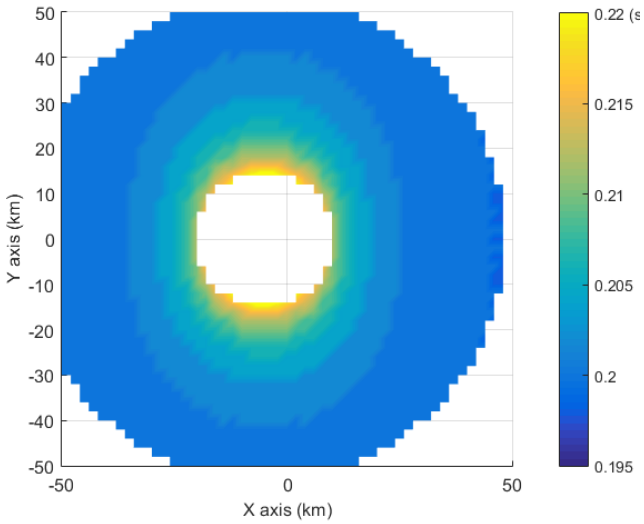

Figure 1. Maximum coherent integration time according to the constraint in (3) with a target velocity magnitude of 100 m/s.

As is apparent, even considering a medium target velocity, the high range resolution amplifies range migration occurrence thus limiting the CIT to approximately 0.2 s throughout the considered area. Obviously, this limit further decreases as the target velocity modulus increases.

It can be shown that this limit can be well approximated by resorting to a first order Taylor expansion of $R_B(t)$. To this purpose we write

$$R_B(t) = \sum_{k=0}^{k=+\infty} \alpha_k t^k \tag{5}$$

where compact explicit expressions can be found for the coefficients up to the second order. Specifically, by defining $\boldsymbol{d}_{TX} = \boldsymbol{P}_{TX} - \boldsymbol{P}(0)$ and $\boldsymbol{d}_{RX} = \boldsymbol{P}_{RX} - \boldsymbol{P}(0)$, we have:

$$\alpha_0 = \|\boldsymbol{d}_{TX}\| + \|\boldsymbol{d}_{RX}\| = R_B(0) \tag{6}$$

$$\alpha_1 = -\left[\frac{\boldsymbol{d}_{TX}}{\|\boldsymbol{d}_{TX}\|} + \frac{\boldsymbol{d}_{RX}}{\|\boldsymbol{d}_{RX}\|}\right]\boldsymbol{v} = -2cos\frac{\beta_0}{2}\boldsymbol{n}_\perp\boldsymbol{v} \tag{7}$$

where β_0 is the bistatic angle (namely the angle between the vectors $\boldsymbol{d}_{TX}$ and $\boldsymbol{d}_{RX}$) and $\boldsymbol{n}_\perp$ is the normal unit vector to the local tangent plane to the bistatic ellipsoid at the target position $\boldsymbol{P}(0)$.

Therefore, as expected, the first order coefficient α_1 is linearly dependent on the radial velocity component of the target, i.e. $V_{rad} = \boldsymbol{n}_\perp\boldsymbol{v}$.

For the second order term we have:

$$\alpha_2 = \frac{1}{2}\left(\frac{1}{\|\boldsymbol{d}_{TX}\|} + \frac{1}{\|\boldsymbol{d}_{RX}\|}\right)\|\mathbf{v}\|^2 - \frac{1}{2}\left[\frac{(\boldsymbol{d}_{TX}\boldsymbol{v})^2}{\|\boldsymbol{d}_{TX}\|^3} + \frac{(\boldsymbol{d}_{RX}\boldsymbol{v})^2}{\|\boldsymbol{d}_{RX}\|^3}\right] \cong \frac{2cos^2\frac{\beta_0}{2}(\boldsymbol{n}_\parallel\boldsymbol{v})^2}{R_B(0)} \tag{8}$$

where the last approximation applies for moderate bistatic angles and target velocity with a dominant cross-range component, , i.e. $V_{cross} = \boldsymbol{n}_\parallel\boldsymbol{v}$.

As previously mentioned the limit on the CIT is mostly due to the first order term in eq. (5), in other words $\Delta R_B(T_{CIT}) \cong \alpha_1 T_{CIT}$ so that $\bar{T}_{CIT}^{(R)} \cong \frac{\Delta R_{res}}{\alpha_1 K}$. This is shown in Figure 2 where the limit CIT evaluated for the first order term of (5) (see blue curve) is compared to the limit CIT arising from the terms of higher orders (see black discontinuous curve). The limits are reported as functions of the target velocity modulus $\|\mathbf{v}\|$. Specifically, for each $\|\mathbf{v}\|$ value, the worst case (i.e. the tightest constraint on the CIT) is reported for any possible target position across the region considered in Figure 1, and for any possible velocity direction ϕ. For instance, by considering the linear term only, with $\|\mathbf{v}\|$=100 m/s, the tightest limit on the CIT is 0.198 s which is well in line with the result in Figure 1. In contrast, the higher order terms would provide a limit CIT of about 7 s.

The comparison between the two curves mentioned above clearly shows that the range migration effect has a linear trend up to CIT in the order of several seconds: at that point also the higher order terms have to be taken into account as they would provide significant migration.

This on one hand demonstrates that the linear range migration effect has to be properly corrected aiming at increasing the CIT with respect to the tight limits in Figure 1 and Figure 2. On the other hand, the comparison above shows that a range migration technique able to compensate only for a linear range variation term would be sufficient in the considered application and, in principle, would allow the CIT to be extended up to a few seconds.

For the sake of completeness, it has to be mentioned that, when increasing the CIT up to a few seconds in the considered application, also the Doppler walk effect has to be taken into account, which is mostly due to the derivative of the second order term of (5). The corresponding limit can be evaluated as:

$$\bar{T}_{CIT}^{(D)} = \max\left\{T_{CIT} \;\middle|\; \Delta f_D(T_{CIT}) < \frac{1}{KT_{CIT}}\right\} \tag{9}$$

being the Doppler resolution inversely proportional to the CIT and indicating with Δf_D the maximum Doppler variation during the CIT. The corresponding limit is reported in Figure 2 for a carrier frequency of 600 MHz and clearly shows that the CIT could be bounded to fraction of seconds for high enough target

This article has been accepted for publication in a future issue of this journal, but has not been fully edited. Content may change prior to final publication. Citation information: DOI 10.1109/TAES.2017.2775924, IEEE Transactions on Aerospace and Electronic Systems

speed even in the absence of accelerations. Therefore, under specific conditions, the Doppler migration compensation would be also required in order to benefit of a CIT in the order of seconds. However, notice that, with reference to Doppler migration, the tightest constraint on the CIT is typically experienced for target moving along the cross-range direction and, when this is the case also the target instantaneous Doppler bandwidth limit has to be considered. In fact, increasing the CIT to a few seconds by compensating for the Doppler migration, would provide the capability to form cross-range profiles for the considered targets (i.e. to resolve different scatterers constituting the target) rather than to enhance the global SNR [26]. For instance, the limit CIT provided by this effect is shown in Figure 2 for a target of length 40 m (see the green curve). As is apparent, in the considered case study, the use of a CIT of about 1 s would yield a limited advantage for detection purposes for a target speed higher than 100 m/s in the cross-range direction. In these conditions, a hybrid coherent/non-coherent integration strategy would be preferable.

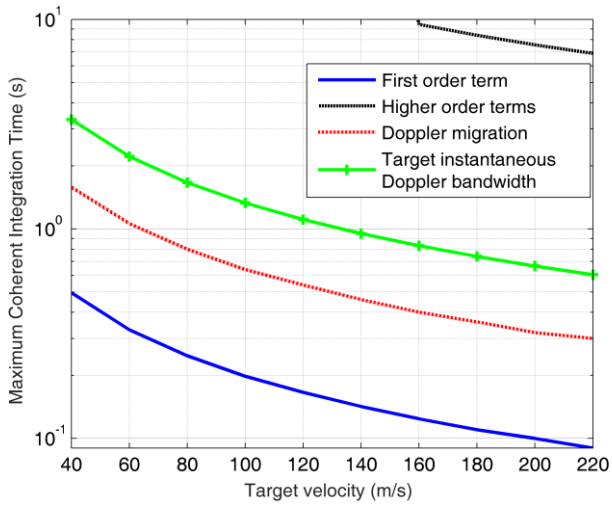

Figure 2. Maximum coherent integration time vs target velocity magnitude based on different constraints for a target belonging to a circular area surrounding the receiver with diameter 100 km.

In this paper we focus mainly on targets with a dominant radial velocity component and we aim to remove the severe limitation imposed by the range walk effect in order to exploit CIT in the order of 1 second.

As a reference, Figure 3 illustrates the result of (1) for 0.9 s CIT for the same geometry of Figure 1 when a target is present at $\boldsymbol{P}(0) = [18\ km, 0, 0]^T$ moving at 200 m/s along the x-axis. The obtained output has been normalized to the maximum expected peak value that is equal to 69.1 dB in the considered case study. As is apparent, with a conventional CAF processing, the target response, while correctly centered, is spread over multiple range bins (about $\frac{2\|\mathbf{v}\|T_{CIT}}{\Delta R_{res}} = 9.1$) and corresponding Doppler bins so that a loss of about 19 dB is measured at the peak location with respect to the maximum expected value.

Therefore, we look for an appropriate and cost-effective approach to compensate for the first order range migration of aerial targets.

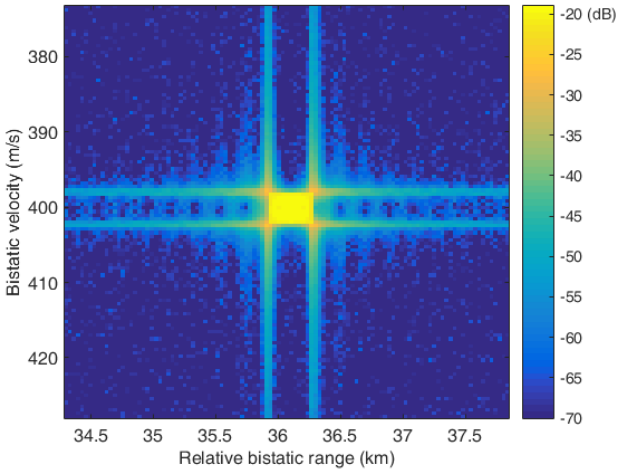

Figure 3. Cross ambiguity function evaluated for a single target at $\boldsymbol{P}(0) = [18\ km, 0, 0]^T$ moving at 200 m/s along the x-axis.

III. Range Migration Compensation via Keystone Transform in Passive Radar

The KT is a well-known technique employed in active pulsed radar system in order to compensate for the range migration of target echoes across consecutive pulses [12]-[14].

It can be successfully applied to passive radar systems employing continuous wave (CW) transmissions by resorting to a batches approach [22]-[23] to recreate the classical slow-time/fast-time framework of a pulsed radar operating at a given PRF. Specifically, the received signals are subdivided into N_B batches of L_B samples each (with $L_B N_B = N_{CIT}$) and the CAF in (1) is rewritten as:

$$\chi[l,m] = \sum_{n=0}^{N_B-1} \sum_{q=0}^{L_B-1} s[nL_B+q]\, r^*[nL_B+q-l] \cdot \exp\left[-j2\pi \frac{m(nL_B+q)}{N_{CIT}}\right] \quad (10)$$

where the index n defines the slow-time domain and the index q indicates the fast-time. For batches dimensions L_B small enough, the compensation of the Doppler induced linear phase term within each batch can be neglected so that the above expression is approximated as:

$$\chi[l,m] = \sum_{n=0}^{N_B-1} \exp\left[-j2\pi \frac{mn}{N_B}\right] \cdot \sum_{q=0}^{L_B-1} s[nL_B+q]\, r^*[nL_B+q-l] \quad (11)$$

When a target is present, moving at limited speed (namely in the absence of range migration within the CIT), the approximation above yields a SNR loss that can be controlled by properly selecting the batches length L_B:

This article has been accepted for publication in a future issue of this journal, but has not been fully edited. Content may change prior to final publication. Citation information: DOI 10.1109/TAES.2017.2775924, IEEE Transactions on Aerospace and Electronic Systems

$$L_{SNR} = -20\,log_{10}\left|\frac{1}{L_B}\frac{sin\left(\frac{\pi m}{N_B}\right)}{sin\left(\frac{\pi m}{N_{CIT}}\right)}\right| \tag{12}$$

Notice that the inner summation in (11) represents the cross-correlation function $\rho_B^{(n)}[l]$ between the surveillance and the reference signals extracted at the *n*-th batch. It can be evaluated at FFT speed by Fourier transforming both fragments and then computing the inverse Fourier Transform of their conjugate product. To this purpose, in order to avoid the border effects due to the FFT-based cyclic cross-correlation, the reference signal batches are partially overlapped by extending each batch by N_τ samples, being N_τ the maximum number of range bins to be included in the final map; accordingly the surveillance signals batches are properly zero-padded with N_τ leading zeros [23].

The expedients above make this Batches Algorithm (BA) of high practical interest especially for passive radar exploiting wider bandwidth signals (e.g. DVB-T transmissions) for which the real-time implementation of (1) is definitely unfeasible.

In the presence of a target moving at high speed, range walk effects will appear as its echoes migrate along the delay (fast-time) dimension across consecutive batches (slow-time).

In particular, assuming that the surveillance signal only contains the returns from a point-like target with unitary amplitude and bistatic velocity linear law given by $R_B(t) = \alpha_0 + \alpha_1 t$, the output of (11) can be written as:

$$\chi_{tgt}[l,m] = \sum_{n=0}^{N_B-1} \exp\left[-j2\pi\frac{mn}{N_B}\right]\exp\left[j2\pi\,\frac{\alpha_1}{\lambda}nT_B\right] \cdot \rho_{ref}^{(n)}\left[l - \frac{\alpha_0+\alpha_1 nT_B}{c}f_s\right] \tag{13}$$

where λ is the wavelength, c is the light speed, $T_B = \frac{L_B}{f_s}$ is the batch duration being f_s the sampling frequency, and we further assumed that the range walk within each batch is negligible so that $\rho_{ref}^{(n)}\left[l - \frac{\alpha_0+\alpha_1 nT_B}{c}f_s\right]$ represents the reference signal auto-correlation function at the *n*-th batch centered at the current target bistatic delay. This range walk is responsible for the coherent integration gain loss observed in Figure 3.

As is apparent, $\chi_{tgt}[l,m]$ is the result of a discrete Fourier transform applied against the columns of the $N_B \times L_B$ slow-time/fast-time data matrix:

$$D[n,l] = \rho_{ref}^{(n)}\left[l - \frac{\alpha_0+\alpha_1 nT_B}{c}f_s\right]\exp\left[j2\pi\frac{\alpha_1}{\lambda}\frac{nL_B}{f_s}\right] \qquad n = 0,..,N_B-1, l = 0,\dots,L_B-1 \tag{14}$$

in order to evaluate the Doppler filters output.

Aiming at compensating the range migration in (13)-(14), the KT operates in the fast-time Fourier transformed (namely the fast-frequency) domain, where the data matrix $D[n,l]$ can be expressed as:

$$D_{ft-FT}[n,p] = P_{ref}^{(n)}[p]\exp\left[j2\pi\frac{p}{T_B}\frac{\alpha_0}{c}\right]\exp\left[j2\pi np\frac{\alpha_1}{c}\right] \exp\left[j2\pi nf_C\frac{\alpha_1}{c}T_B\right] \tag{15}$$

where $P_{ref}^{(n)}[p]$ is the Fourier transformed auto-correlation of the reference signal, namely the power spectral density of the signal estimated at the *n*-th batch.

The first exponential factor in (15) accounts for the target distance at the initial batch and yields a linear phase term along the fast-frequency dimension; the third exponential factor reflects the Doppler induced linear phase shift of the carrier $f_C = c/\lambda$ across consecutive batches. The second exponential factor is the one encoding the range migration effect as it jointly depends on the batch number *n* and on the fast-frequency index p (i.e. on the frequency component displacement, $\Delta f_p = \frac{p}{T_B}$, with respect to the carrier frequency f_C).

As it is well known, the KT compensate for this term by rescaling the slow-time (i.e. interpolating the slow-time samples sequences) according to the following rule:

$$\bar{n} = \frac{f_C+\Delta f_p}{f_C}n \tag{16}$$

and this leads to:

$$D_{ft-FT}[\bar{n},p] = P_{ref}^{\left(\frac{f_C}{f_C+\Delta f_p}\bar{n}\right)}[p]\ \exp\left[j2\pi\frac{p}{T_B}\frac{\alpha_0}{c}\right]\exp\left[j2\pi\bar{n}f_C\frac{\alpha_1}{c}T_B\right] \tag{17}$$

that approximately resembles the fast-time Fourier transformed data matrix for a non-migrating target echo. Therefore, after a fast-time inverse Fourier Transform and a slow-time Fourier Transform, the bistatic range/Doppler map is obtained with range migration correction for any given target bistatic velocity.

However, we observe that a resampled version of $P_{ref}^{(n)}[p]$ is exploited after the time scaling. Notice that, in conventional pulsed radar, this function would be independent of *n* as the radar transmits a train of identical pulses. In passive radar, the spectral shape of the waveform of opportunity might change on consecutive batches depending on the signal modulation and on the batches temporal separation. Therefore, the resulting amplitude modulation has to be carefully considered to avoid the formation of artifacts in the resulting range-Doppler map. This undesired effect can be again controlled by acting on the batch duration. Specifically, it has to be selected so that the possible variation of $P_{ref}^{(n)}[p]$ across the slow-time is sufficiently slow, i.e. $P_{ref}^{\left(\frac{f_C}{f_C+\Delta f_p}\bar{n}\right)}[p] \cong P_{ref}^{(\bar{n})}[p]$. As an alternative, a reciprocal filter could be employed at the range compression stage so that the filter impulse response would be constant across consecutive batches [4]. However this would yield additional SNR loss compared to the matched filter approach (namely the cross-correlation between the reference and the surveillance signal fragments).

This article has been accepted for publication in a future issue of this journal, but has not been fully edited. Content may change prior to final publication. Citation information: DOI 10.1109/TAES.2017.2775924, IEEE Transactions on Aerospace and Electronic Systems

Figure 4 sketches the main steps of the KT for passive radar system based on a batches architecture. It includes the same processing blocks required for its application to active pulsed radar. However, according to the discussion above, this scheme is effective in the passive radar case employing CW transmissions if all the following conditions hold:

1) the batches duration T_B is selected so as to limit the SNR loss due to the neglect of the Doppler induced linear phase term within the batch ('Doppler assumption').
2) A 'stop&go' approximation applies along the slow-time dimension, i.e. the target range migration within the batch is negligible ('stop&go assumption'). Again, this sets an upper constraint to the batches duration T_B.
3) The signal of opportunity has slowly varying spectral characteristics compared to the batch duration ('stationary signal assumption').

The first point applies also to the basic BA without range migration compensation whereas the latter two points are specific of the KT.

It is also worth noticing that the first two approximations are commonly adopted also in conventional pulsed radar systems. However, in that case, the validity of these assumptions is largely guaranteed by the small duty-cycle, namely the ratio between the pulse duration and the pulse repetition time.

In passive radar exploiting continuous signals, the slow-time/fast-time framework is recreated based on a signal fragmentation that intrinsically yields a 100% duty-cycle. However, the above conditions can be reasonably controlled by limiting the batches duration as this is not subject to other severe constraints.

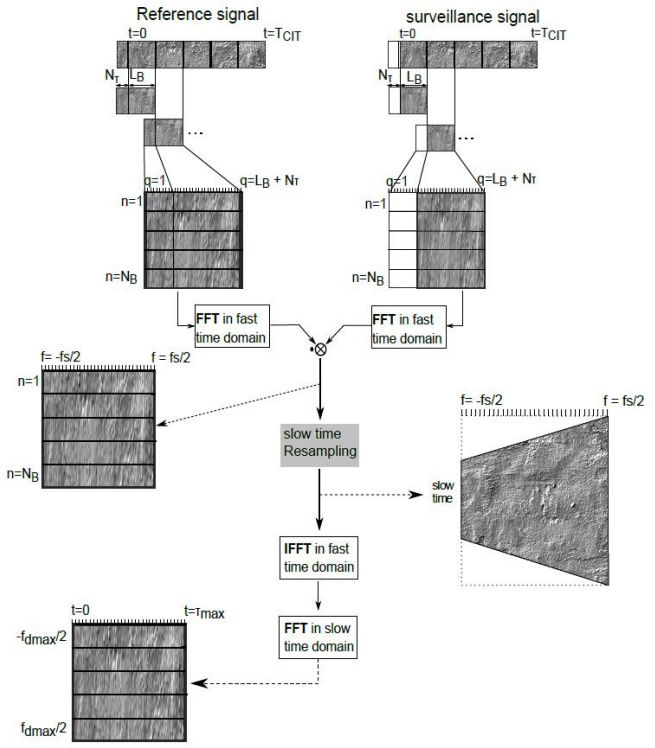

Figure 4. Bistatic range/Doppler map evaluation in passive radar system with a batches architecture based Keystone Transform for range migration compensation.

In particular, reducing the batch duration T_B is expected to progressively improve the performance based on the three conditions above while it only affects the computational load of the processing, especially when a KT is employed.

Notice that, compared to the basic BA without range migration compensation, the KT just requires one additional processing block, i.e. that devoted to the slow-time resampling (see the grey block in Figure 4). However, this is a computationally intensive processing stage as it has to be performed at each fast-frequency bin. Therefore, in the next section, we consider and compare efficient methods to obtain the required slow-time rescaling.

IV. Alternative Slow-Time Interpolation Methods and Adopted Metrics

Different approaches have been devised aiming at reducing the computational load of the KT slow-time resampling stage with respect to a conventional SCI [17][21][24][25].

With particular reference to the PR case, in [21] the CZT was adopted thanks to its capability to limit the computational complexity while providing optimal performance. Specifically, the CZT-based KT for a PR exploiting DVB-T transmissions is fully described in [21] and its performance is characterized both in terms of computational load, possible hardware implementation, and via application to an experimental data registration. The results show that the CZT provides an invaluable tool for practical implementation of the KT in DVB-T based PR that possibly allows a real-time operation, depending on the considered processing unit. Incidentally we observe that, by using the CZT, the last FFT block in Figure 4 is not strictly required [21] since the transform can directly provide the slow-time interpolated results in the Doppler domain. Actually, this expedient allows a significant computational load saving with only a limited border effect on the employed CIT that could be responsible of modified sidelobes structures in the final range/Doppler map. In the following we use a biased point of view that favors the CZT-based solution; specifically this fast CZT-based KT implementation will be considered when evaluating the computational load but the border effect will be neglected when investigating the achievable results.

In this paper we consider an alternative interpolation method that exploits Lagrange *P*-order polynomials aiming at further reducing the computational load of the slow-time resampling stage of the KT.

The *P*-LPI based resampling of (15) according to (16) can be readily obtained as:

$$D_{ft-FT}[\bar{n},p] = \sum_{n=\lceil \bar{n}-(P+1)/2 \rceil}^{\lfloor \bar{n}+(P+1)/2 \rfloor} D_{ft-FT}[n,p] \left(\prod_{m=0, m\neq n}^{P} \frac{\bar{n}-n}{n-m} \right) \quad (18)$$

where *P* is the order of the polynomial adopted and $D_{ft-FT}[n,p]$ is the slow-time/fast-frequency data matrix in (15).

Basically, only *P*+1 consecutive samples in the slow-time

This article has been accepted for publication in a future issue of this journal, but has not been fully edited. Content may change prior to final publication. Citation information: DOI 10.1109/TAES.2017.2775924, IEEE Transactions on Aerospace and Electronic Systems

domain are exploited to evaluate each interpolated sample according to a *P*-order polynomial. Accordingly, this method is expected to allow a significant reduction of the computational load when reducing the order of the polynomial. However, it is intrinsically sub-optimal as it implements a very local interpolation of the available slow-time sequences and its performance is expected to get worse as P decreases. Specifically, this might yield both SNR loss and the presence of artifacts in the final range/Doppler map that possibly jeopardize the useful target echo detection against noise.

Nevertheless, it is interesting to observe that for PR exploiting CW transmissions, the equivalent slow-time sampling rate (namely the PRF) can be adjusted to partially correct interpolation mistakes. In other words, it is expected that a lower order LPI could be exploited with negligible loss when shorter batches durations T_B are adopted and this is well in line with the constraints posed by the conditions listed in Section III (i.e. Doppler, stop&go, and stationary signal assumptions). Clearly, the reduction of T_B has to be traded for a possibly higher computational load since it would affect the global number of slow-time samples.

As mentioned in the introduction, possible application of the P-LPI for the active radar case has been preliminary investigated in [25] while only the case of a linear interpolation (namely a 1-LPI) has been recently considered for the PR case in [17].

Therefore, in this paper, we extend these studies by investigating the suitability of the generic P-LPI-based KT for the PR case. The aim is to provide a thorough comparison with other interpolation methods as well as proper indications on the selection of the relevant parameters.

To this purpose, we adopt a set of appropriate metrics to evaluate the impact of different interpolation methods on the final result on the range/Doppler map as well as their effectiveness to compensate for target range migration.

The adopted metrics are defined assuming that a single point-like target is present and are listed in the following. We will refer to the illustrative example reported in Figure 5 where the CZT-based KT has been applied against the same case considered in Figure 3.

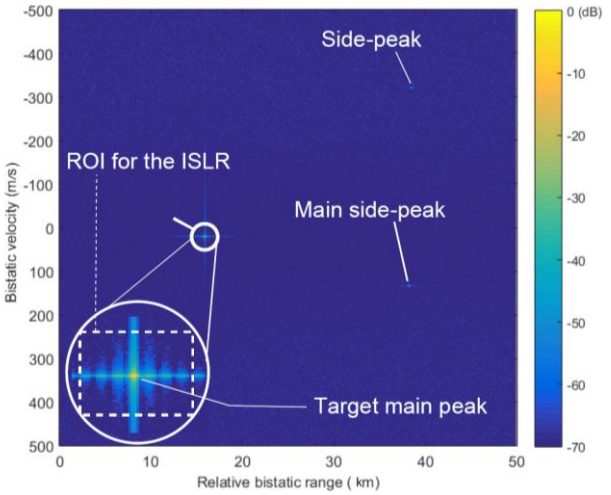

Figure 5. Illustration of the adopted metrics on the bistatic range-velocity plane.

- **Target peak loss**. This parameter measures the loss experienced at the target location on the final range/Doppler map with respect to its nominal expected value in the absence of range migration. Specifically, it is defined as:

$$P_{Loss} = -20log_{10}\left(\frac{1}{N_{CIT}}\left|\chi\left[l_{tgt}, m_{tgt}\right]\right|\right) \quad (19)$$

where $[l_{tgt}, m_{tgt}]$ are the target coordinates on the range/Doppler plane and N_{CIT} is the maximum expected peak value after coherent integration in the absence of migration using the conventional CAF. As is apparent, this definition also includes the loss due to the batches architecture (see (12)). Therefore it will be useful to understand the additional loss due to the selected interpolation method.

The following three metrics are intended to analyze the sidelobes level in the final range/Doppler map in order to highlight the presence of artifacts or spurious peaks caused by the application of the considered approach. They are defined with reference to different regions of the map.

- **Peak to side lobe ratio (PSLR)**. This parameter measures the level of the highest secondary peak appearing in the range/Doppler map and compares it to the main peak at the target location:

$$PSLR = 20log_{10}\left(\frac{\left|\chi\left[l_{tgt}, m_{tgt}\right]\right|}{\left|\chi[l_{SL}, m_{SL}]\right|}\right) \quad (20)$$

When DVB-T signals are exploited together with proper tapering functions to limit the sinc-shaped sidelobes, this parameter will be mostly affected by the presence of specific features in the OFDM modulation that yield a number of undesired side-peaks in signal ambiguity function [5]. However, when the KT is employed, the final range/Doppler map might show a modified PSLR value depending on the batches architecture parameters and on the effectiveness of the interpolation stage.

- **Integrated side lobe ratio (ISLR)**. This parameter is defined as the ratio of the total power in all side lobes contained in a specific region of interest (ROI) to the power in main lobe, and is expressed as:

$$ISLR = 10log_{10}\left(\frac{\int_{(x,y)\in ROI}|\chi(x,y)|^2 dxdy)}{\int_{(x,y)\in Main\ lobe}|\chi(x,y)|^2 dxdy}\right) \quad (21)$$

We focus on a small region surrounding the target main peak where the nominal signal ambiguity function shows the typical two dimensional sinus cardinal shape. Therefore, the ISLR provides indication about the masking effect of a strong target on weak targets in the neighborhood. Specifically, in this study, the ROI is centered at target peak location and its size is set to 20

This article has been accepted for publication in a future issue of this journal, but has not been fully edited. Content may change prior to final publication. Citation information: DOI 10.1109/TAES.2017.2775924, IEEE Transactions on Aerospace and Electronic Systems

m/s in velocity dimension (at a carrier frequency of 600 MHz) and 2 km in range dimension (see Figure 5).
To provide a similar measure on a wider region we also introduce the

- **Global integrated side lobes ratio (GISLR)**. This parameter is defined as:

$$GISLR = 10log_{10}\left(\frac{\int_{(x,y)\in MAP}|\chi(x,y)|^2 dxdy)}{\int_{(x,y)\in Main\ lobe}|\chi(x,y)|^2 dxdy}\right) \quad (22)$$

where the integrated sidelobe level is evaluated on the whole range/Doppler map considered for the PR application. In this study we consider a range/Doppler map extension corresponding to 50 km × 1000 m/s at a carrier frequency of 600 MHz (see Figure 5).

Finally, in order to analyze the computational complexity yield by different algorithms, we further consider among the adopted metrics, the

- **Computational load**. This is evaluated in this study as the number of complex multiplications required by the considered approach. The results obtained as a function of the relevant parameters are reported in Table 1 for the BA (without range migration compensation) compared to the KT based on efficient slow-time interpolation methods. Besides the expected dependence on the number of batches N_B and their length L_B, the computational load of the different approaches also depends on the number N_τ of delay bins included in the range/Doppler map.

TABLE 1 - COMPUTATIONAL LOAD EVALUATED FOR ALTERNATIVE ALGORITHMS FOR RANGE-DOPPLER MAP EVALUATION

Batches Algorithm	$N_B\left[3(L_B+N_\tau)log_2(L_B+N_\tau)+L_B+N_\tau\left(1+log_2(N_B)\right)\right]$
CZT-based KT	$N_B\left[3(L_B+N_\tau)log_2(L_B+N_\tau)+L_B+N_\tau\right]+(L_B+N_\tau)\left[4N_B+2N_B\left(1+3log_2(2N_B)\right)\right]$
P-LPI based KT	$N_B\left[3(L_B+N_\tau)log_2(L_B+N_\tau)+L_B+N_\tau\left(1+log_2(N_B)\right)\right]+N_B(L_B+N_\tau)\left((P+1)2P\right)$

V. COMPARISON OF DIFFERENT INTERPOLATION METHODS

The metrics introduced in the previous section are evaluated in the following for different algorithms applied against simulated data accounting for a single point-like target. Specifically, we consider a CIT of 0.9 s and a target echo with initial bistatic range equal to 26 km and constant bistatic velocity equal to 400 m/s (corresponding to a target flying at 200 m/s along a radial direction). Therefore, a range migration across about 10 range cells is expected during the CIT in the absence of corrections.

The main objective of this analysis is to compare the theoretical performance of alternative interpolation methods for KT in passive radar. Moreover we aim at identifying possible degradations with respect to the ideal case without range migration so that we can understand which is the unavoidable price to be paid in order to obtain the sought migration correction. With particular reference to the proposed *P*-LPI method, we also aim at assessing the achievable performance for different choices of the relevant parameters, i.e. the polynomials order *P* and the batches duration, in order to provide practical indications to the interested reader.

Figure 6 reports the target peak loss obtained with various algorithms as a function of the batches length L_B. Specifically the results for the SCI-based KT and the CZT-based KT are compared to the loss measured with the *P*-LPI based KT with different choices of the polynomial order *P* (i.e. *P*=1, 3, 5, and 7).

In addition, the result obtained with the BA in the absence of range migration is also reported for comparison. The corresponding curve is obtained by eq. (12) and represents the lowest bound for the different KT versions. In fact, it encodes the loss due to the batches architecture, namely the loss due to the 'Doppler assumption', which increases as the batches get longer.

The curves in Figure 6 confirm that both the SCI and the CZT based interpolation are optimum methods as they do not yield additional loss with respect to the BA operating in the ideal case (no range migration). This is tantamount to say that both the SCI-based KT and the CZT-based KT provide an effective compensation of the range migration by focusing all the target energy at the expected range-Doppler location.

This is not an obvious result in the passive radar case because of the 'stop&go assumption' and the 'stationary signal assumption' discussed in Section III. Specifically, with reference to the first assumption, we observe that with a sampling frequency of $\frac{64}{7}$ MHz ≅ 9.14 MHz, the considered L_B values spans a batches duration interval between 110 μs and 450 μs.

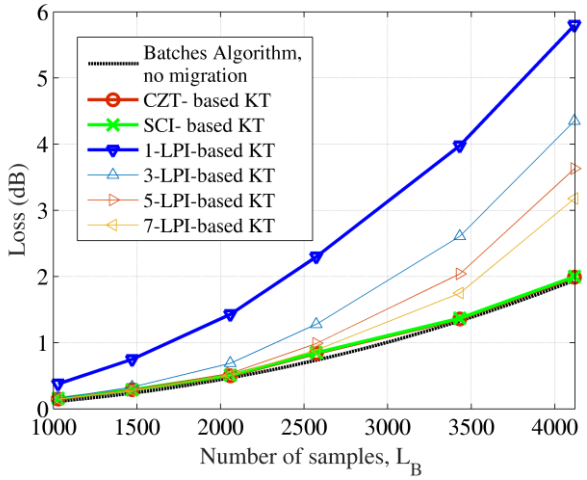

Figure 6. Comparison of target peak loss obtained for different algorithms as a function of the batches length.

This article has been accepted for publication in a future issue of this journal, but has not been fully edited. Content may change prior to final publication. Citation information: DOI 10.1109/TAES.2017.2775924, IEEE Transactions on Aerospace and Electronic Systems

Therefore, the expected range migration within each batch is about 18 cm in the worst case, which clearly shows that the 'stop&go assumption' is indeed valid within the considered interval.

As regards the 'stationary signal assumption', we notice that we exploited a *8k* DVB-T transmission mode so that the OFDM symbol duration is $T_u = 896\mu s$, plus a guard interval of 1/32. With the considered L_B values, the batches duration is always supposed to be a fraction of T_u so that the same OFDM symbol spans over multiple batches. Consequently, the employed signal can be assumed to show slowly varying characteristics across the slow time samples, i.e. $P_{ref}^{\left(\frac{f_C}{f_C+\Delta f_p}\bar{n}\right)}[p] \cong P_{ref}^{(\bar{n})}[p]$ in eq. (17).

The curves obtained for the different versions of the *P*-LPI based KT clearly show that the expected target peak loss is a function of both the batches length L_B and the polynomial order *P*. Specifically, as for the SCI and the CZT interpolation methods, the loss increases as the batches are extended. However, due to the sub-optimality of the P-LPI method, additional target peak loss are observed with respect to the ideal BA. This clearly shows that, with certain selections of its parameters, the *P*-LPI method fails at totally recovering the target energy spread over multiple range cells.

Nevertheless we notice that the derivative of the loss curve with respect to L_B increases as *P* decreases. In other words, in order to limit the loss to a given acceptable value, shorter batches are required when low order polynomials are exploited at the interpolation stage. As an example, by setting the maximum loss to 0.8 dB, a batches length L_B=2500 can be exploited with the SCI and the CZT, the 3-LPI would require L_B=2200, while using a linear interpolation (1-LPI) limits the batches length to L_B=1500. Interestingly enough, for any given acceptable loss, it is possible to identify a proper combination of L_B and *P* so that the *P*-LPI method could accomplish the requirement.

Similar considerations apply to the performance comparison reported in Figure 7. Specifically Figure 7(a-c) show the results obtained with different methods for the three metrics related to the sidelobes level in the final range/Doppler map, namely the PSLR, the ISRL, and the GISLR, respectively. In each figure, most of the reported curves show increasing values as the batch duration increases. This possibly proves the insurgence of artifacts or spurious peaks caused by the application of the considered approach, there including the batches strategy and the range migration compensation stage. Incidentally we observe that the ISLR (Figure 7(b)) is less sensitive to the batch duration showing quite constant values for many of the methods adopted in the considered study case.

The SCI-based KT and the CZT-based KT yield identical curves and are shown to be the best performing methods for the considered interval of L_B values. In contrast, the *P*-LPI method might cause a slight increase in the sidelobes level, with reference to both the highest side-peak and the average sidelobes surrounding the main peak in the range-Doppler plane. However, there exist choices of L_B and *P* that guarantee a proper control of the sidelobes level. Therefore, even a simple linear interpolation (i.e. 1-LPI) can be exploited if the batches length can be kept sufficiently small. For instance, the 1-LPI based KT with L_B=1500 provides similar performance with respect to the CZT-based KT with L_B=2500.

Based on the analysis above, the performance degradation yield by the sub-optimum *P*-LPI method can be largely controlled by properly selecting both the order *P* of the polynomial and the system equivalent PRF.

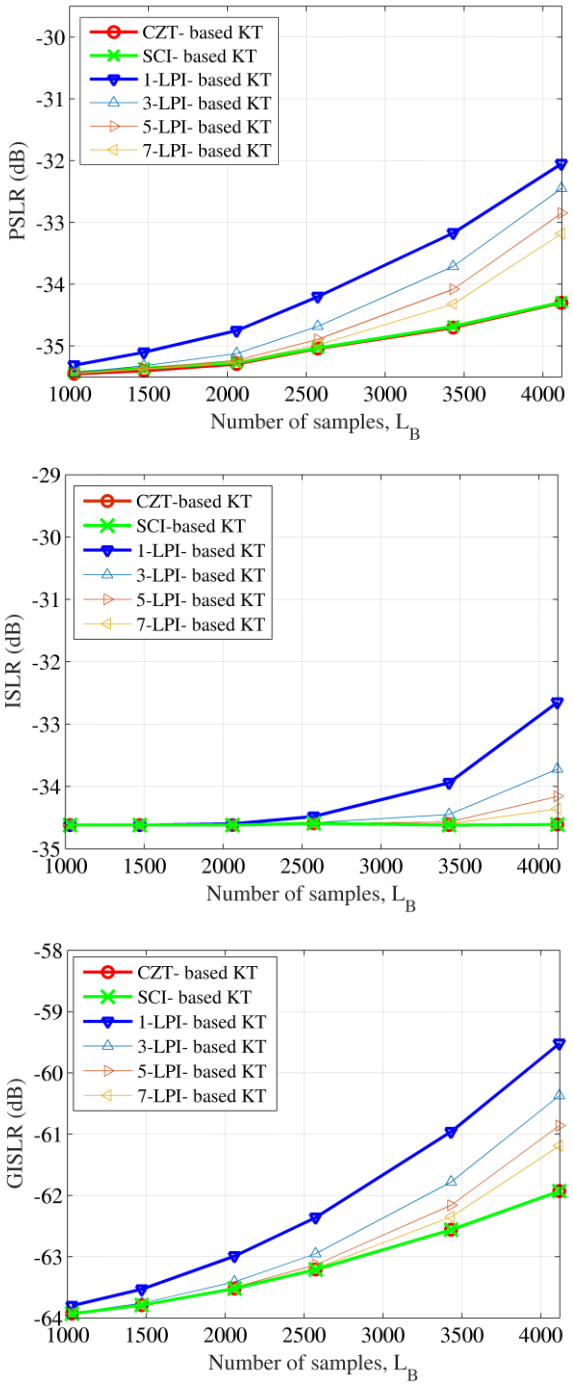

Figure 7. Comparison of the sidelobes level in the final range-Doppler map obtained for different algorithms as a function of the batches length: (a) Peak to side lobe ratio (PSLR); (b) Integrated side lobe ratio (ISLR); (c) Global integrated side lobes ratio.

This article has been accepted for publication in a future issue of this journal, but has not been fully edited. Content may change prior to final publication. Citation information: DOI 10.1109/TAES.2017.2775924, IEEE Transactions on Aerospace and Electronic Systems

In this regard, the *P*-LPI method appears as an effective solution for the PR case since it provides a flexible tool to be employed within a KT stage. In fact, in PR system, the equivalent PRF resulting from the batching strategy is not subject to severe constraints on range and Doppler ambiguities. In contrast its setting is typically regulated by the requirements on SNR loss and computational load [22]-[23].

Therefore, it is possible to identify proper choices for this parameter so that, even operating with the *P*-LPI with a limited order *P*, negligible loss should be accepted with respect to the application of a SCI or a CZT based interpolations. Moreover, the expected loss can be traded for a reduced computational load.

In order to investigate the computational efficiency of the proposed interpolation method, Figure 8 reports the computational load required by different algorithms as a function of the number of samples in each batch, L_B. To this purpose we assumed that the CIT is 0.9 s and the maximum bistatic range of interest is 130 km, which yields $N_d = 3659$ samples in the range dimension.

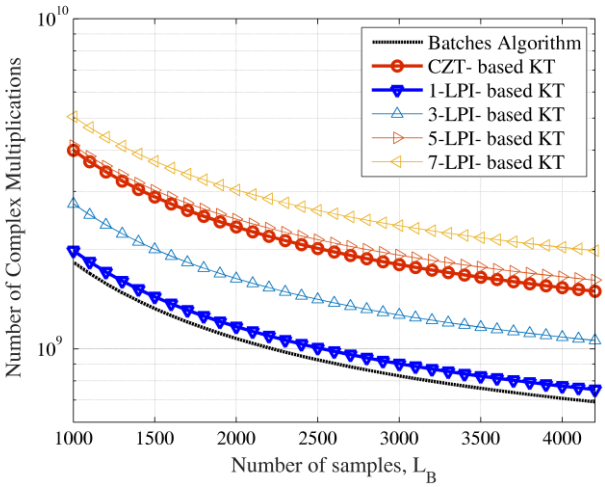

Figure 8. Comparison of the computational load required by different algorithms as a function of the batches length.

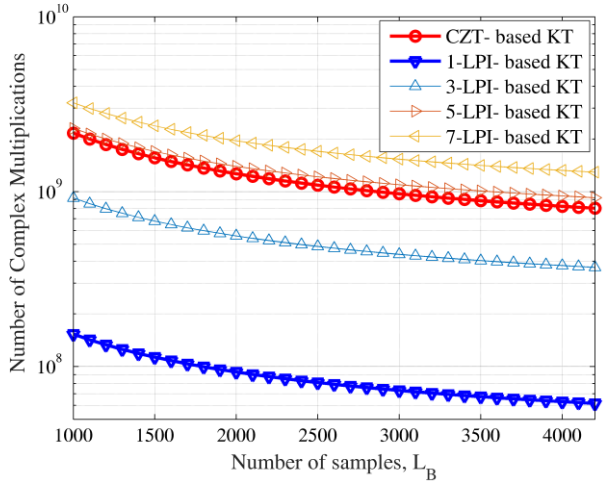

Figure 9. Comparison of the computational load required as an extra to batch algorithm by different algorithms as a function of the batches length.

As expected, all the considered methods show a computational complexity that decreases as the batches duration increases. The BA without range migration compensation provides the lowest computational load that in turn represents the lowest bound to the complexity of any considered method based on such fundamental architecture. The capability to compensate the target range migration is paid in term of additional complex multiplications, as required by the slow-time interpolation stage of the KT. However, by exploiting different interpolation approaches, the experienced increase in computational complexity might significantly vary.

Specifically, the CZT-based KT yields a number of complex multiplications more than doubled with respect to the BA for convenient values of L_B. A similar result is obtained when operating with a *P*-LPI method with a high polynomial order *P* (i.e. $P \geq 5$ in the considered case). In contrast, by reducing *P*, the *P*-LPI based KT allows to limit the additional computational complexity required to achieve the desired range migration compensation. Particularly, the 1-LPI method only requires a slight increase in the computational load with respect to the BA.

For the sake of fairness, the comparison above should be repeated under the constraint of a similar coherent integration loss (see Figure 6). However we observe that, even in that case, similar considerations hold. For instance, with a maximum loss to 0.8 dB, the CZT-based KT with L_B=2500 would require a number of complex multiplications 1.4 times higher than the 1-LPI based KT with L_B=1500. Moreover we observe that the setting of the polynomial order in principle provides a greater flexibility in the trade-off between performance and computational complexity.

Again we recall that the computational load saving cannot be by orders of magnitude since the complexity is lower bounded by the computational load of the standard BA without range migration compensation. This is quite apparent in Figure 9 where we compare just the additional computational load required by different implementations of the KT. In particular one might notice that this additional cost with the 1-LPI based KT is one order of magnitude smaller than with the CZT-based KT.

Finally, we observe that, being based on few consecutive slow-time samples, the *P*-LPI based KT method intrinsically operate in a sequential manner against the received data. In other words, the interpolation stage can be started after the reception of the first *P*+1 batches and can be operated sliding across the slow-time domain. As a consequence the required processing can be easily pipelined with the previous stages devoted to the computation of the cross-correlation between the reference signal and the surveillance signal performed on a batch basis (see Figure 4). Similarly, the output of the interpolation can be readily fed as input to the IFFT going back into the fast-time domain. In contrast, a CZT-based approach would require all the batches in the CIT to be available at the receiver in order to provide the final output in a parallel manner. Therefore, in that case, the additional computations required by the KT would start after the reception of the whole CIT with a resulting intrinsic latency.

This article has been accepted for publication in a future issue of this journal, but has not been fully edited. Content may change prior to final publication. Citation information: DOI 10.1109/TAES.2017.2775924, IEEE Transactions on Aerospace and Electronic Systems

VI. Results against experimental data

In this section, we show the benefits of the proposed range migration compensation techniques against experimental data collected by a DVB-T based PR for an aerial surveillance scenario.

A. Acquisition campaign and adopted methodology

The data sets exploited in this paper have been provided by Leonardo S.p.A. in the framework of a long-term collaboration with the research group at Sapienza University of Rome. In the considered data acquisition campaign, the DVB-T based PR receiver was fielded at the Leonardo premises, in Rome (see Figure 10).

It featured two surveillance antennas displaced in the horizontal plane. The antennas were pointed at 270° clockwise from North so as to include in their 36° main beam many civilian air traffic routes departing or arriving to the Fiumicino and Ciampino airports. Depending on the considered test, the reference antenna was steered toward the DVB-T transmitter of Monte Cavo or Monte Guadagnolo (see Figure 10) to collect the DVB-T channels emitted at a carrier frequency of 762 MHz and 482 MHz, respectively.

Different data sets have been collected for a total acquisition time of 156 minutes. In detail, each data set is composed by consecutive data files, namely scans, spaced by 7 s.

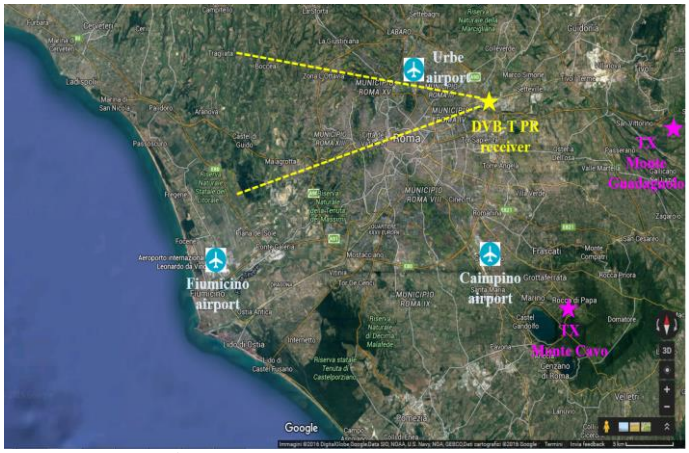

Figure 10. Sketch of the acquisition geometry.

All the available data files have been processed according to the DVB-T PR processing scheme developed by the authors and presented in [5][8]. Specifically, the removal of the undesired contributions in the surveillance channel, i.e. direct signal and multipath echoes, is performed via the sliding version of the extensive cancellation algorithm (ECA-S) [27]. This operates over a range of 33 km (1000 taps @ fs=64/7 MHz) with a batch duration equal to 0.1 s whereas the filter update rate is 13 ms. Then, the reference signal is properly pre-filtered to remove the high side-lobes and spurious peaks appearing in the DVB-T signal ambiguity function. To this purpose, we resort to the linear approach presented in [5] which is based on the cascade of the pilots signals equalization and a residual peaks removal (RPR) filter to mitigate the zero-Doppler peaks.

Successively, the mismatched reference signal and the output signals from the ECA-S filter are jointly exploited to achieve coherent integration on CIT of about 1-2 s. To this purpose, different algorithms have been considered.

Firstly, the conventional CAF in (1) has been evaluated, without range migration compensation, by resorting to the Correlation FFT algorithm [22] which is the most efficient solution for the CAF formation when DVB-T signals are exploited. Notice that the conventional CAF represents the upper bound on SNR when no migration effects are present since no SNR loss is introduced. In addition, a 1-LPI-based-KT and a CZT-based-KT with batch length L_B=1715 have been considered for range migration compensation.

Once the bistatic range-velocity maps have been evaluated at both surveillance channels, a conventional Cell Average Constant False Alarm Rate (CA-CFAR) threshold is separately applied to each map to detect targets with a probability of false alarm equal to $P_{fa} = 10^{-3}$. A two-out-of-two criterion is adopted to integrate the detection results obtained at the two surveillance channels allowing a nominal $P_{fa} = 10^{-6}$ on the final range-velocity plane.

Live Air Traffic Control (ATC) registrations of the corresponding aircrafts of the same area have been also collected. This allowed us to carry out a quantitative analysis to evaluate the target detection improvement resulting from the correction of its range migration when long integration times are considered. In fact, we have evaluated the number of correct detections resulting from the application of the different approaches for all the targets of opportunity included in the available air-truth. Specifically, we define a given detection as "correct" when it appears at both expected range-velocity location and expected time instant. All the remaining plots are then labeled as false alarms.

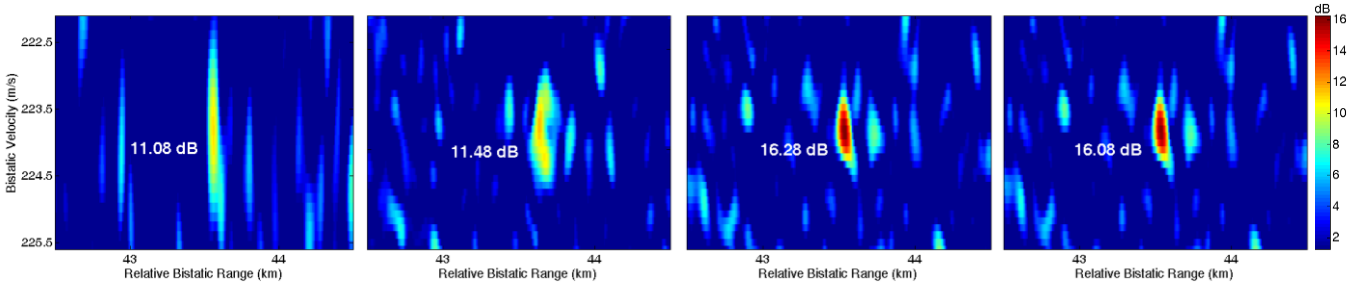

(a) (b) (c) (d)

Figure 11. Enlarged views of the range-velocity maps obtained with different algorithms for a target with a dominant motion component along the range dimension. (a) Conventional CAF with CIT=0.3 s; (b) Conventional CAF with CIT =1 s; (c) 1-LPI-based-KT with CIT=1 s; (d) CZT-based-KT with CIT=1 s.

This article has been accepted for publication in a future issue of this journal, but has not been fully edited. Content may change prior to final publication. Citation information: DOI 10.1109/TAES.2017.2775924, IEEE Transactions on Aerospace and Electronic Systems

An extensive analysis on the available data sets is reported in the following sub-section.

B. *Target detection performance analysis*

To readily understand the effects of different approaches for range-velocity map evaluation, Figure 11 reports an enlarged view of the results obtained on a single scan for a target with a dominant motion component along the range dimension. All the reported results have been normalized to the thermal noise power level so that each value represents the estimated SNR. The real target is moving around the bistatic location with coordinates [43.5 km, 224 m/s]. When a conventional CAF map is evaluated with a CIT=0.3 s (see Figure 11(a)), a reasonably narrow peak is formed in the range dimension as the range walk effects are negligible. In contrast, when we extend the CIT up to 1 s (Figure 11(b)), a range spreading is clearly visible in the conventional CAF map. As a consequence, a SNR improvement of just fractions of dB is measured at the peak location with respect Figure 11(a). When applying the KT based range migration compensation, the benefits of an extended CIT are apparent. This is illustrated in Figure 11(c)-(d) where a 1-LPI-based KT and a CZT-based KT have been considered, respectively. Interestingly enough, the two algorithms provide largely comparable outputs. In fact, in both cases, the target's echo appears well focused in range and velocity dimensions. Correspondingly, a SNR improvement of about 5 dB is obtained with respect to both Figure 11(a) and Figure 11(b) and this clearly reveals the successful exploitation of a CIT more than tripled.

Figure 12 reports the detection results obtained across the 42 scans belonging to the same test considered in Figure 11. Specifically, Figures 12(a-d) have been obtained with the same approaches adopted in Figures 11(a-d). In each figure, colored or gray dots have been employed to plot the raw detections of the PR sensor while in black we reported the available ATC registrations for comparison. In order to obtain much clearer outputs, all the plots within a bistatic range of 6 km have been discarded.

The detections appearing within the first 14 km (surrounded by the green rectangle in Figure 12(a)) correspond to vehicles moving on the highway near the receiver position, [28]. Instead, the plots between 16 and 35 km (surrounded by the orange rectangle in Figure 12(a)) correspond to aircrafts, devoid of ADSB transponder, that are landing or taking off from the small civilian Urbe airport situated near the Leonardo premises (see Figure 10).

The remaining targets have been grouped into two classes:

(i) high bistatic velocity targets, that, based on the motion model adopted in Section II, are expected to move with a dominant motion component along the range dimension thus yielding an approximately constant bistatic Doppler during the CIT (see for example the target track with red dots in Figure 12(a)), and

(ii) low bistatic velocity targets that obviously yield a limited range migration during the CIT but can be rather affected by Doppler migration (see for example the target track with blue dots in Figure 12(a)).

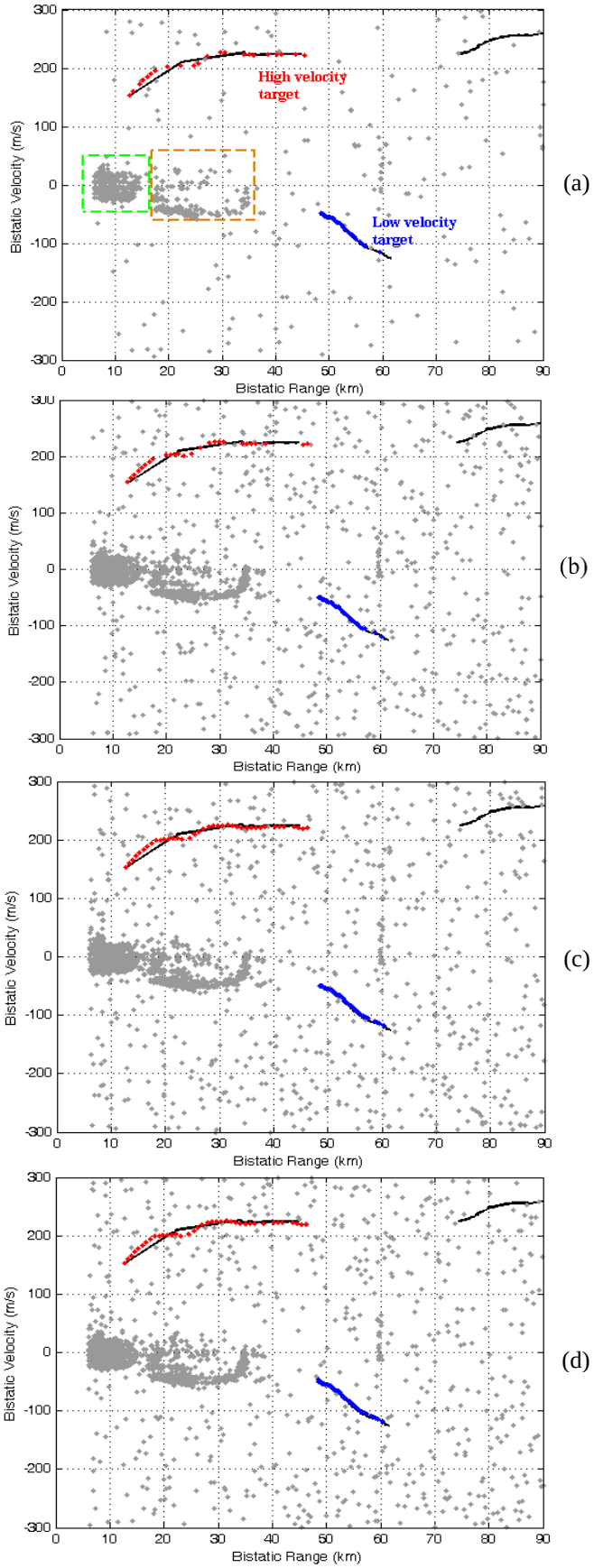

Figure 12. Detection results across 42 consecutive scans when using different algorithms. (a) Conventional CAF with CIT=0.3 s; (b) Conventional CAF with CIT=1 s; (c) 1-LPI-based KT with CIT=1 s; (d) CZT-based KT with CIT=1 s.

This article has been accepted for publication in a future issue of this journal, but has not been fully edited. Content may change prior to final publication. Citation information: DOI 10.1109/TAES.2017.2775924, IEEE Transactions on Aerospace and Electronic Systems

We expect that the first class includes the targets that are the most interesting ones to show the benefits of the considered range migration compensation approaches.

In fact, we observe from Figure 12, that the target appearing at low bistatic velocity is almost continuously detected with all the considered approaches (a few additional missed detections are experienced when operating with a CIT=0.3 s, as in Figure 12(a)). In contrast, from Figure 12(a)-(b) we notice that, if no range migration compensation is performed, a discontinuous plot sequence is obtained for the target at high bistatic velocity when the CIT is equal to 0.3 s or 1 s, respectively.

As it is apparent, the increase of the integration time does not provide a significant improvement in term of target detection capability. In fact, the number of correct detections moves from 22 to 26 (over 42) when we extend the CIT from 0.3 s to 1 s. In contrast, many additional plots are obtained when the proposed 1-LPI-based KT is applied (see Figure 12(c)) against a CIT=1 s. Noticeably, similar results are achieved with the CZT-based KT (Figure 12(d)) despite the additional computational load. In particular, for the considered target, the number of correct detections is equal to 39 and 38 when operating with the 1-LPI-based KT and the CZT-based KT approaches, respectively. In other words, the target is rather continuously detected all along the acquisition time.

A more extensive analysis along this line is reported in Table 2 for a different test that included many targets of opportunity within the first 80 km of bistatic range. Specifically, the columns of Table 2 report the number of correct detections of each target of opportunity included in the available air truth when different algorithms and CIT durations are considered. The maximum number of possible detections for each target has been also reported. The same target classification discussed above has been adopted to easily identify the targets that are worth the application of the range migration compensation algorithms. In detail, in the present analysis, a target is labeled as a high (H) or low (L) velocity target at the scans where it is observed with bistatic velocity greater or lower than 125 m/s, respectively. According to this criterion, a given target track is typically subdivided into two portions belonging to the different regions.

In the penultimate columns of Table 2 we have evaluated the total number of correct detections for the two target classes, obtained as a summation of the detections for all the targets belonging to the considered class. Finally, the estimated false alarm rate is reported in the last column of Table 2; this is obtained by evaluating the number of false alarms (e.g. scattered grey plots in Figure 12) and averaging over a bistatic range-velocity region where no target is expected to fall. An indication of the margin of error is also shown for a confidence coefficient of 0.95. As is apparent, in all cases, the estimates of the false alarm rate are only slightly higher than the nominal value of the P_{fa} equal to 10^{-6}.

Focusing on the target detection capability, we observe that when we limit the CIT to 0.3 s, the detection results are comparable for the different processing schemes, namely the conventional CAF, the 1-LPI-based KT and the CZT-based KT.

This result holds also when longer CIT are used if low bistatic velocity targets are considered. As expected the capability of detecting such targets increases with the CIT duration. However it is not enhanced by the range migration compensation stage at least up to the considered CIT values.

In contrast, a significant improvement is obtained in term of target detection capability for high velocity targets by exploiting the algorithms including a range migration compensation stage. Notice that, for such targets, the use of a longer CIT might even provide some detection losses when a conventional CAF is applied (see for example Targets 1-5). This is reasonably attributed to the masking effect yield by the target energy spreading around the cell under test (see Figure 11(b)).

When a range migration compensation stage is included, the number of correct detections is largely enhanced. With

Table 2. Detection results obtained against a single data set when different CAF algorithms and different integration time values are considered.

Cases		Targets of opportunity														Total detections		Etimated false alarm rate
		Target 1		Target 2		Target 3		Target 4		Target 5		Target 6		Target 7		High velocity targets	Low velocity targets	
n° of possible detections		H 33	L 34	H 31	L 33	H 34	L 21	H 35	L 44	H 15	L 25	H 14	L 20	H 17	L 21	179	197	
CIT=0.3 s	Optimum CAF	7	21	10	20	13	13	6	19	3	15	2	14	2	15	43	117	$3.8\cdot10^{-6} \pm 2.3\cdot10^{-7}$
	1-LPI- based-KT	8	20	9	22	15	12	6	18	3	15	2	14	2	16	45	117	$3.7\cdot10^{-6} \pm 2.3\cdot10^{-7}$
	CZT-based-KT	8	20	9	22	15	12	6	18	3	15	2	14	2	16	45	117	$3.7\cdot10^{-6} \pm 2.3\cdot10^{-7}$
CIT=1 s	Optimum CAF	13	28	10	25	10	18	8	26	4	22	6	16	2	17	53	152	$4.1\cdot10^{-6} \pm 1.3\cdot10^{-7}$
	1-LPI- based-KT	15	29	12	26	19	17	13	31	9	22	10	17	3	17	81	159	$4.1\cdot10^{-6} \pm 1.3\cdot10^{-7}$
	CZT-based-KT	17	29	12	25	19	16	13	31	10	22	10	17	2	17	83	157	$4.0\cdot10^{-6} \pm 1.3\cdot10^{-7}$
CIT=2 s	Optimum CAF	4	29	7	29	8	19	2	28	2	21	6	18	2	21	31	165	$4.2\cdot10^{-6} \pm 9.5\cdot10^{-8}$
	1-LPI- based-KT	14	30	17	31	22	18	13	31	14	23	8	17	3	19	91	169	$4.1\cdot10^{-6} \pm 9.4\cdot10^{-8}$
	CZT-based-KT	16	31	16	31	21	18	13	31	14	23	10	16	5	20	95	170	$4.1\cdot10^{-6} \pm 9.4\cdot10^{-8}$

This article has been accepted for publication in a future issue of this journal, but has not been fully edited. Content may change prior to final publication. Citation information: DOI 10.1109/TAES.2017.2775924, IEEE Transactions on Aerospace and Electronic Systems

reference to the global number of correct detections, when CIT=2 s, the number of correct detections provided by the CZT-based KT algorithm (95) is approximately tripled with respect to the conventional CAF (31).

Table 2 clearly shows that the 1-LPI-based KT technique provides comparable results with respect to the CZT-based KT algorithm for all the reported targets of opportunity. This in turn demonstrates that the intrinsic approximations of this low order *P*-LPI-based KT do not significantly affect the final performance with respect to the use of a conventional optimum resampling stage within the KT.

Notice that, although the target detection capability of high velocity targets is significantly enhanced when the proposed techniques are exploited, the achieved probability of detection is still limited (95 correct detections are obtained out of the 179 maximum possible detections achievable). This is possibly due to the high altitudes of such fast moving targets whose detection could be limited by the vertical-plane radiation patterns of DVB-T transmitters. In addition, Doppler migration effects cannot be excluded for these targets and the compensation of such effects requires additional processing stages not included in the proposed schemes.

The analysis above has been further extended by summing up the results from to all the available data sets. Following the adopted target classification, Table 3 reports the overall number of correct detections evaluated for all the targets of opportunity included in each data set, distinguishing between high bistatic velocity targets and low bistatic velocity targets. The same combinations of algorithms and CIT values of Table 2 have been included in the reported analysis.

Again, the joint exploitation of long CIT and range migration compensation techniques yields a remarkable enhancement in target detection performance. This is clearly apparent from the last three rows of Table 3 (based on a CIT of 2 s).

Specifically, for targets moving at low bistatic velocity, the use of a long CIT (up to the considered values) allows an enhancement of targets detection capability also when a conventional processing is applied. However, even in this case, the application of range migration compensation techniques guarantees an increased continuity in the obtained plot sequences. For instance, when CIT=2 s, an improvement of about 5% is obtained using the 1-LPI-based KT and the CZT-based KT with respect to the conventional CAF.

For high velocity targets, the exploitation of a range migration compensation stage together with a long CIT allows a number of correct detections approximately doubled with respect to the results obtained with the same approach against short CIT=0.3 s. In other words, the considered range migration compensation stage allows to effectively exploit the increased CIT duration.

In contrast, we might observe that when a conventional CAF is employed, the increase of the integration time up to 2 s yields a slight degradation of the detection performance. As previously mentioned, this is also a consequence of the target's echo spreading across range and Doppler that might jeopardize the effectiveness of a CA-CFAR detection scheme.

Consequently, the advantage of the proposed scheme over a conventional CAF progressively enhances as the adopted CIT increases. In this regard we observe that both the 1-LPI-based KT and the CZT-based KT with CIT=2 s yield a 67% increase in the number of correct detections with respect to the best result obtained with the conventional CAF operating with CIT=1 s.

Finally, based on the results above, it is evident that the proposed *P*-LPI-based KT operating with *P*=1 provides the same detection results obtained with the CZT-based KT while reducing the computational load of the resulting system.

VII. Conclusions

In this paper, an alternative interpolation strategy is proposed to implement the slow time resampling stage required by the KT algorithm for range migration compensation. The proposed approach is intended to provide a low cost solution to be fruitfully employed in passive radar based on transmissions of opportunity with reasonably wide frequency bandwidth.

Specifically, based on a batches architecture, we resort to a Lagrange *P*-order polynomial interpolation and we verify that the proposed approach might represent a flexible tool to be employed within a KT stage for passive radar. In fact, whilst this method is intrinsically sub-optimal, we show that the expected loss can be largely controlled by properly selecting the relevant parameters of the algorithm thus trading the achievable performance for a reduced computational load. Specifically, by properly acting on the batches duration, we show that, even operating with a limited order *P*, negligible loss should be accepted with respect to other interpolation approaches, with a corresponding computational load saving.

The practical effectiveness of the proposed scheme is demonstrated by extensive application against experimental data sets provided by Leonardo S.p.A..

Table 3. Synthesis of the detection results obtained against all the available data sets.

		High velocity targets	Low velocity targets
Possible detections		943	1441
CIT = 0.3 s	**Optimum CAF**	175	875
	1-LPI- based-KT	190	875
	CZT-based-KT	190	877
CIT = 1 s	**Optimum CAF**	229	1069
	1-LPI- based-KT	312	1112
	CZT-based-KT	306	1107
CIT = 2 s	**Optimum CAF**	161	1141
	1-LPI- based-KT	383	1203
	CZT-based-KT	386	1198

References

[1] Griffiths, H. D., and Baker, C. J., "Passive coherent location radar systems. Part 1: Performance prediction.", IEE Proceedings on Radar, Sonar and Navigation, 152, 3 (June 2005), 153—159.

[2] Christiansen, J. M., Olsen, K. E., and Weiß, G.,"Coherent range and Doppler-walk compensation in PBR applications," 2014 15th International Radar Symposium (IRS), Gdansk, 2014, pp. 1-4.

[3] Christiansen, J. M., and Olsen, K. E., "Range and Doppler walk in DVB-T based Passive Bistatic Radar," 2010 IEEE Radar Conference, Washington, DC, 2010, pp. 620-626.

[4] Palmer, J. E., Harms, H. A., Searle, S. J., and Davis, L. M.,"DVB-T Passive radar Signal Processing". IEEE Trans. on Signal Processing, April 2013.
[5] Colone, F., Langellotti, D., and Lombardo, P.,"DVB-T signal ambiguity function control for passive radars". IEEE Transactions on Aerospace and Electronic Systems, January 2014.
[6] Kuschel, H., Heckenbach, J., O'Hagan, D., Ummenhofer, M., "A hybrid multi-frequency Passive Radar concept for medium range air surveillance", 2011 Microwaves, Radar and Remote Sensing Symposium (MRRS), pp.275-279, 25-27 Aug. 2011.
[7] Kulpa, K., Malanowski, M., Misiurewicz, J., Samczynski, P.,"Passive radar for strategic object protection", 2011 IEEE International Conference on Microwaves, Communications, Antennas and Electronics Systems (COMCAS), pp. 1-4.
[8] Martelli, T., Colone, F., Tilli, E., and Di Lallo A., "Multi-frequency target detection techniques for DVB-T based passive radar sensors", Sensors, vol. 16, no. 10, article n. 1594, 2016.
[9] Kulpa, K. S. and Misiurewicz, J.,"Stretch Processing for Long Integration Time Passive Covert Radar," *2006 CIE International Conference on Radar*, Shanghai, 2006, pp. 1-4.
[10] Malanowski, M., Kulpa, K. and Olsen, K. E., "Extending the integration time in DVB-T-based passive radar," *2011 8th European Radar Conference*, Manchester, 2011, pp. 190-193.
[11] Radmard, M., Habibi, H., Bastani, M. H. and Behnia, F., "Target's range migration compensation in passive radar," *2009 European Radar Conference (EuRAD)*, Rome, 2009, pp. 457-460.
[12] Li, Y., Zeng, T., Long, T., and Wang, Z., "Range Migration Compensation and Doppler Ambiguity Resolution by Keystone Transform", Proceedings Intl. Conf. on Radar 2006 (CIE 2006), pp. 1 – 4, 2006.
[13] Perry, R.P., Di Pietro, R.C., and Fante, R.L., 'SAR imaging of moving targets', IEEE Trans. Aerosp. Electr. Syst., 1999, 35, (1), pp. 188–200.
[14] Perry, R. P., Di Pietro, R. C., and Fante, R. L., "Coherent Integration With Range Migration Using Keystone Formatting", Proceedings 2007 IEEE Radar Conference, pp. 863 – 868, 2007.
[15] Liu, L., Tao, R., and Zhang, N., "The CAF-DFRFT-KT Algorithm for High-Speed Target Detection in Passive Radar," 2011 First International Conference on Instrumentation, Measurement, Computer, Communication and Control, Beijing, 2011, pp. 748-751.
[16] Feng, Y., Shan, T., Zhuo, Z., and Tao, R., "The migration compensation methods for DTV based passive radar," 2013 IEEE Radar Conference (RadarCon13), Ottawa, ON, 2013, pp. 1-4.
[17] Guan, X., Zhong, L., Hu, D., and Ding, C., "An extended processing scheme for coherent integration and parameter estimation based on matched filtering in passive radar", Journal of Zhejiang University SCIENCE C, 2014, Volume 15, Number 11, Page 1071.
[18] Barott, W. C. and Engle, J., "Single-antenna ATSC passive radar observations with remodulation and keystone formatting," 2014 IEEE Radar Conference, Cincinnati, OH, 2014.
[19] Scott, K. M., Barott, W. C. and Himed, B., "The keystone transform: Practical limits and extension to second order corrections," 2015 IEEE Radar Conference (RadarCon), Arlington, VA, 2015.
[20] Bai, X., Feng, Y., and Zhao, J., "A processing scheme for long integration time passive radar based on CZT and FRFD-sharpness," 2016 IEEE International Conference on Signal Processing, Communications and Computing (ICSPCC), Hong Kong, 2016, pp. 1-4.
[21] Shan, T., Liu, S., Zhang, Y. D., Amin, M. G., Tao, R. and Feng, Y., "Efficient architecture and hardware implementation of coherent integration processor for digital video broadcast-based passive bistatic radar," IET Radar, Sonar & Navigation, vol. 10, no. 1, pp. 97-106, 1 2016.
[22] Lombardo, P., and Colone, F., "Advanced processing methods for passive bistatic radar systems," in *Principles of Modern Radar: Advanced Radar Techniques*, W. L. Melvin, and J. A. Scheer, Raleigh, NC: SciTech Publishing, 2012.
[23] Moscardini, C., Petri, D., Capria, A., Conti, M., Martorella, M., and Berizzi, F., "Batches algorithm for passive radar: a theoretical analysis," in *IEEE Transactions on Aerospace and Electronic Systems*, vol. 51, no. 2, pp. 1475-1487, April 2015.
[24] Wang, Y., Li, J.W., Chen, J., Xu, H.P., and Sun, B., 'A parameter-adjusting polar format algorithm for extremely high squint SAR imaging', IEEE Trans Geosci. Remote Sens., 2014, 52, (1), pp. 640–650.
[25] Deng, T., and Jiang, C., "Evaluations of keystone transforms using several interpolation methods," Proceedings of 2011 IEEE CIE International Conference on Radar, Chengdu, 2011, pp. 1876-1878.
[26] Colone, F., Pastina, D., and Marongiu, V., "VHF Cross-Range Profiling of Aerial Targets Via Passive ISAR: signal processing schemes and experimental results", IEEE Trans. on Aerospace and Electronic Systems.
[27] Colone, F., Palmarini, C., Martelli, T. and Tilli, E., "Sliding extensive cancellation algorithm for disturbance removal in passive radar," in *IEEE Transactions on Aerospace and Electronic Systems*, vol. 52, no. 3, pp. 1309-1326, June 2016.
[28] Langellotti, D., Sedehi, M., Colone, F. and Lombardo, P.,"Experimental results for passive bistatic radar based on DVB-T signals," 2013 14th International Radar Symposium (IRS), Dresden, 2013, pp. 178-183.

Florian Pignol received the Master degree in General Engineering from Ecole Centrale de Marseille University, Marseille, France, in September 2016.

From June to November 2014 he had the opportunity to work on acoustics field at Microflown Technologies, The Netherlands. From April to December 2016 he was a visiting student at Sapienza University of Rome where he focused his activity on passive radar system.

From April 2017 he is an Engineer at Satellogic, Argentina.

Fabiola Colone received the laurea degree (B.S.+M.S.) in Communication Engineering and the Ph.D. degree in Remote Sensing from the University of Rome "La Sapienza", Rome, Italy, in 2002 and 2006, respectively.

She joined the INFOCOM Dept., University of Rome "La Sapienza", Italy, as a Research Associate in January 2006. From December 2006 to June 2007, she was a Visiting Scientist at the Electronic and Electrical Engineering Dept. of the University College London, London, U.K. She is currently an Associate Professor at the DIET Department of the University of Rome "La Sapienza" where she teaches courses on radar topics.

Dr. Colone's current research interests include passive coherent location (PCL), multi-channel adaptive signal processing, and space-time adaptive processing (STAP) with application to mono- and bi-static radar systems. Her research in these areas has been reported in over 100 publications in international technical journals, book chapters, and conference proceedings. The research experience of Dr. Colone in these fields is also demonstrated by the participation, with scientific responsibility roles, in research projects funded by the European Union, the European Defence Agency, the Italian Space Agency, the Italian Ministry of Research, and the radar industry.

She is member of the AESS Board of Governors for the three-year term 2017-2019 and IEEE Senior Member. She is Associate Editor for the IEEE Transactions on Signal Processing since January 2017 and member of the Editorial Board of the International Journal of Electronics and

Communications (AEÜ) (Elsevier) since October 2011. She was in the organizing committee, as the Student Forum Co-Chair, of the IEEE 2008 Radar Conference, Rome, Italy. She served in the technical committee of many international conferences on radar systems and signal processing, and she is frequently reviewer for a number of international technical journals.

Tatiana Martelli received the Master degree in communication engineering and the Ph.D. degree in Remote Sensing from Sapienza University of Rome, Italy, in 2012 and 2016, respectively.

From March 2016, she has been a PostDoctoral Researcher at the DIET Dept. of Sapienza University of Rome.

She is involved in research projects funded by the European Union and Leonardo. Her research interests include passive radar systems; in particular, her activity is focused on the design of signal processing techniques for detection, localization and imaging of targets.